This measurement was obtained, only in the horizontal plane, by rotating the thruster in 10° increments.

Results and Conclusions

As can be seen in Fig. 3, the peak noise power occurred at ±25° from boresight and was minimal (limited by the 10 db dynamic range of the measurement) at ±90° from boresight. The noise is not polarized; no change in level was observed when rotating the horn on its own axis. The photos in Fig. 3 were obtained by opening the camera lens and allowing 15 firings for each picture. The calibration in these photos is 0.0 dbm = 1 div (5 mv), + 3.0 dbm = 2 div, + 4.2 dbm = 3 div.

These measurements, made in a narrow band of interest at X band, provide data that can be used in the initial design of the LES-7 communication system. These data indicate the noise relative to the thruster; they do not allow for satellite antenna gain characteristics or the coupling of the noise with these antennae. Thus, future measurements will have to be made on the actual satellite antennae models and systems when they become available.

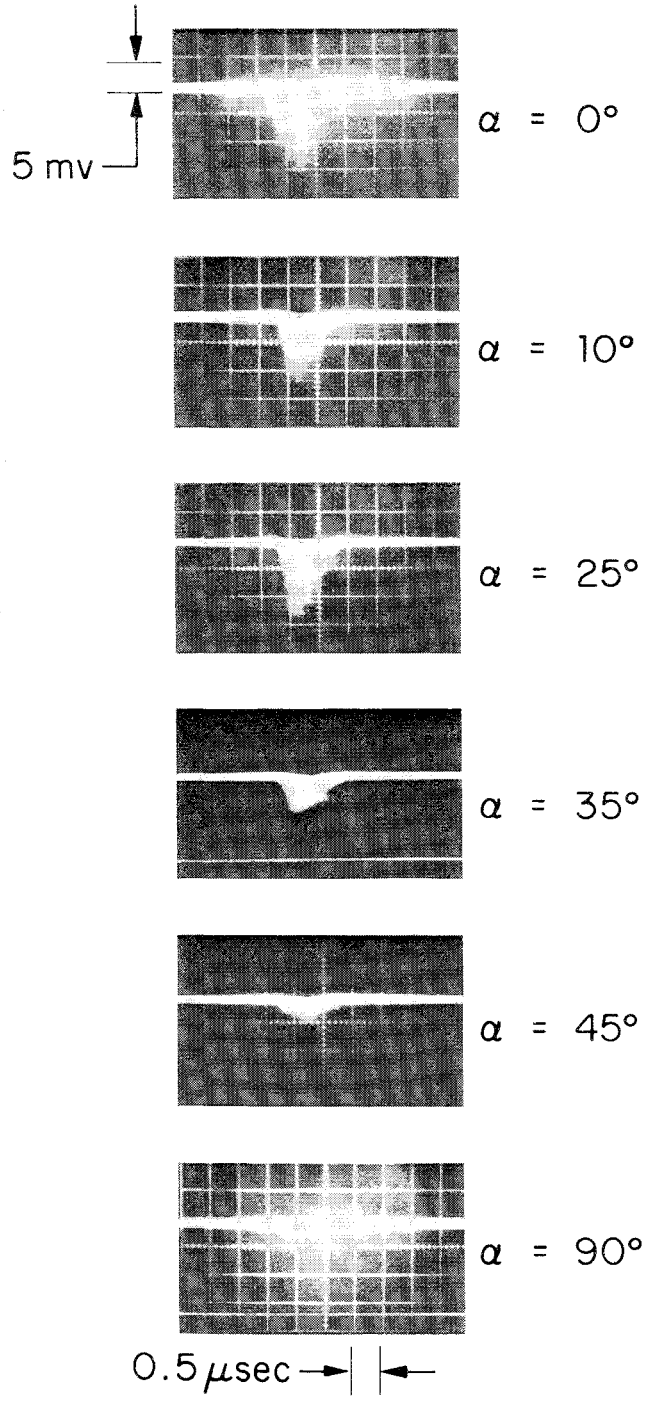

Fig. 3 Measured RFI for various angles α between thruster discharge axis and X-band antenna.

Calculation of Real-Gas Effects in the Depressurization of Air Storage Cylinders

THEO GORDON KEITH JR.*
Naval Ship Research and Development Laboratory, Annapolis, Md.

AND

JAMES E. A. JOHN†
Department of Mechanical Engineering, University of Maryland, College Park, Md.

Nomenclature

A_i = interior surface area of cylinder
$A_i(T)$ = functional relation of temperature dependent density coefficients
A_t = cross-sectional area of nozzle throat
a = speed of sound
a_{ij} = subscripted virial coefficients
c_k = coefficients in the $c_{p,0}$ series of Appendix
c_p = specific heat at constant pressure
$c_{p,0}$ = perfect-gas specific heat at constant pressure
D_i, D_t = inside diameter and throat diameter of cylinder
$f_i(\rho,T)$ = functions of $Z = Z(\rho,T)$, Appendix, i = 1,2,...,6
Gr = Grashof number, $D_i^3\rho^2 g\beta\Delta T/\mu^2$
g = acceleration of gravity
$g_i(T_2,T_1)$ = specific heat functions, Appendix, i = 1,2,3
h = specific enthalpy
h_i = heat-transfer coefficient at interior of cylinder
k_0 = thermal conductivity of flask gas
M_t = Mach number evaluated at nozzle throat
$M_{t,j}$ = jth estimate of M_t (j = I,II,...)
$m, \dot{m}_0$ = mass and mass flow rate of cylinder gas
m_w = mass of cylinder wall
P_{0i} = initial pressure of cylinder gas
Pr = Prandtl number, $c_p\mu/k$
q_i = heat-transfer rate at interior of cylinder
R = gas constant
$R(\rho_t)$ = residual in iteration for ρ_t, Eq. (9)
s = specific entropy
T_{0i} = initial temperature of cylinder gas
$T_{t,j}$ = jth estimate of T_t (j = I,II,...)
U_0, u_0 = total and specific flask gas internal energies
V, v = volume and specific volume
w = velocity
Z = compressibility factor
β_0 = volumetric expansion coefficient of cylinder gas
γ = ratio of specific heats
ϵ = tolerance used for successive approximations
θ, θ_c = time, and critical time required for P_t to reach P_∞
μ_0 = dynamic viscosity of cylinder gas
ρ = density
$\rho_{t,I}, \rho_{t,j}$ = first and jth estimations of ρ_t
$\bar{(\ )}$ = arithmetic average of ( ) over one time interval

Received November 7, 1969; revision received March 9, 1970.

* Mechanical Engineer.

† Professor.

Subscripts

t = nozzle throat
0 = cylinder gas
∞ = ambient
w = internal cylinder wall

Introduction

THE expulsion of a gas from a pressurized reservoir through a valve or nozzle occurs in many industrial and military applications. The importance of heat transfer in the problem depends upon the speed at which the expulsion is made; in situations of extremely rapid blowdown it may be neglected. On the other hand, the frequently employed ideal gas assumption is plausible only if the gas pressures and temperatures are not far removed from atmospheric conditions.

Reynolds and Kays[1] included heat transfer in the blowdown problem, using a lumped method to characterize the gas state, and treating the heat stored in the walls as being concentrated in a simple uniform temperature heat capacitor. Excellent agreement between prediction and experiment was obtained using free convection as a means of heat transport between the gas and cylinder walls. They assumed the gas to be perfect and parametrically analyzed several limiting cases of gas expulsion. Unfortunately, their work only dealt with low pressure situations, and tests were made with $P_{0i} \simeq 100$ psi. The objectives of the present study were to demonstrate analytically how gas imperfections may be accounted for in the blowdown analysis when a gas is allowed to escape through a "choked" nozzle, to determine the limits of applicability of the ideal gas assumption, and to confirm the real gas predictions experimentally.

Method of Analysis

For the consideration of gas imperfections in compressible flow, Tsien[2] proposed a perturbation scheme using van der Waal's equation of state and a quadratic expression for $c_p(T)$. Tao[3] improved on Tsien's method by using the more accurate Beattie-Bridgeman equation of state and a c_p function which also contained pressure. Johnson[4,5] proposed an analytical technique which is quite general and which does not feature long approximate equations; he applied the method to isentropic flow through a nozzle for fixed reservoir conditions. If the reservoir is considered to be finite in size so that the pressure and temperature vary with time, it is seen that Johnson's problem becomes equivalent to the problem of this analysis. The mass flow rate from the flask is $\dot{m}_0 = -dm_0/d\theta$, and an energy balance on the flask gas gives $dU_0 = d(m_0u_0) = q_i d\theta - h_0\dot{m}_0 d\theta$. Combining these equations along with the definition of enthalpy leads to

$$m_0 dh_0 = q_i d\theta + V_0 dP_0 \tag{1}$$

In general, $dh = c_p dT + [v - T(\partial v/\partial T)_p]dP$, so Eq. (1) may be written as

$$m_0 c_p dT_0 = q_i d\theta - (m_0 T_0/\rho_0^2)(\partial\rho_0/\partial T_0)_p dP_0 \tag{2}$$

Now from a general functional expression of state, $F(\rho,T,P) = 0$, the following product may be formed:

$$(\partial\rho/\partial T)_p(\partial T/\partial P)_\rho(\partial P/\partial\rho)_T = -1 \tag{3}$$

But $P = Z\rho RT$, so Eq. (3) becomes

$$(\partial P/\partial T)_\rho = -(\rho/T)\{[Z + T(\partial Z/\partial T)_\rho/[Z + \rho(\partial Z/\partial\rho)_T]\} \tag{4}$$

or, with the functions defined in Appendix

$$(\partial\rho/\partial T)_p = -(\rho/T)[(1 + f_1 + f_2)/(1 + f_3)] \tag{5}$$

Inserting Eq. (5) and the expression for specific heat developed in Johnson into Eq. (2), we obtain

$$dT_0 = \frac{q_i d\theta + (m_0/\rho_0)[(1 + f_1 + f_2)/(1 + f_3)]dP_0}{m_0[c_{p,0}/R + (1 + f_1 + f_2)^2/(1 + f_3) - (1 - f_6)]} \tag{6}$$

Even if the depressurization is adiabatic, Eq. (6) cannot be solved in closed form (as was possible in the perfect gas case), but it may be evaluated by a finite difference scheme using an iterative method (because both sides of the equation depend upon temperature). When the coefficients of the differentials are averaged, Eq. (6) becomes

$$(T_0)_{n+1} = (T_0)_n + \frac{q_i\Delta\theta + V_0[1 + f_1(\bar{\rho}_0,\bar{T}_0) + f_2(\bar{\rho}_0,\bar{T}_0)]\Delta P_0}{\bar{m}_0\left\{\frac{c_{p,0}}{R}(\bar{T}_0) + \frac{[1 + f_1(\bar{\rho}_0,\bar{T}_0) + f_2(\bar{\rho}_0,\bar{T}_0)]^2}{1 + f_3(\bar{\rho}_0,\bar{T}_0)} - [1 + f_6(\bar{\rho}_0,\bar{T}_0)]\right\}} \tag{7}$$

To solve this expression, simultaneous solution of the equations which describe the flow through the nozzle is required. The approach used closely follows Johnson's,[5] except that the reservoir is assumed to have fixed properties (arithmetic mean values) only over a small time interval $\Delta\theta = \theta_{n+1} - \theta_n$. Now, since the flow in the nozzle is presumed isentropic, from the Appendix

$$(s_0 - s_t)/R = 0 = g_1(\bar{T}_0,T_t) + \ln(\rho_t/\rho_0) - f_4(\bar{\rho}_0,\bar{T}_0) + f_4(\bar{\rho}_t,\bar{T}_t) \tag{8}$$

The unknowns in Eq. (8) are T_t and ρ_t. Suppose the first estimate of the throat temperature $T_{t,I}$ is taken as the perfect gas value. Equation (8) can then be written as

$$\ln\left(\frac{\rho_t}{\rho_0}\right) - f_4(\bar{\rho}_0,\bar{T}_0) + f_4(\rho_t,T_{t,I}) + g_1(\bar{T}_0,T_{t,I}) = R(\rho_t) \tag{9}$$

where $R(\rho_t)$ is the residual which must be reduced to zero by proper selection of throat density. In the computer program, Newton's method is used to reduce the residual, i.e.,

$$\rho_{t,II} = \rho_{t,I} - R(\rho_{t,I})/[dR(\rho_{t,I})/d\rho_t]$$

or, with $R(\rho_{t,I})$ given by Eq. (9), using $\ln(\rho_{t,I}/\rho_0)$ as the first term,

$$\rho_{t,II} = \rho_{t,I} - R(\rho_{t,I})\rho_{t,I}/[1 + f_1(\rho_{t,I},T_{t,I}) + f_2(\rho_{t,I},T_{t,I})] \tag{10}$$

The calculation procedure continues until

$$|\rho_{t,II} - \rho_{t,I}| < \epsilon \tag{11}$$

Since the flow is adiabatic, $dh + d(w^2/2) = 0$, and since w_0 is assumed to be zero, then $w_t^2/2 = h_0 - h_t$. Using the enthalpy difference developed in the Appendix results in

$$w_t^2/2 = [1 + f_1(\bar{\rho}_0,\bar{T}_0) - f_5(\bar{\rho}_0,\bar{T}_0)]\bar{T}_0 - [1 + f_1(\rho_t^*,T_{t,I}) - f_5(\rho_t^*,T_{t,I})]T_{t,I} + g_2(\bar{T}_0,T_{t,I}) \tag{12}$$

where ρ_t^* is the throat density which reduced the residual of Eq. (9) for a given $T_{t,I}$. It is assumed that the nozzle is operating in a "choked" condition and hence: $M_t = 1$, $P_t \geq P_\infty$, and $w_t = a_t$, where a_t is taken from Eq. (A17) of the Appendix. If w_t from Eq. (12) is not equal to a_t from Eq. (A17), a new $T_{t,II}$ is estimated in the following way: the perfect gas relation $T_0/T_t = 1 + (\gamma - 1)M_t^2/2$ is used to calculate the change in T_t for a given change of M_t: $(\partial T_t/\partial M_t)_s = -(T_t^2/\bar{T}_0)(\gamma - 1)M_t$. Thus,

$$T_{t,II} = T_{t,I} - (T_{t,I}^2/\bar{T}_0)(\gamma - 1)M_{t,I}(1 - M_{t,I}) \tag{13}$$

Rather than continuously employing Eq. (13) for succeeding estimations, it was found that linear extensions of the most recent calculations gave faster convergence and new estimation

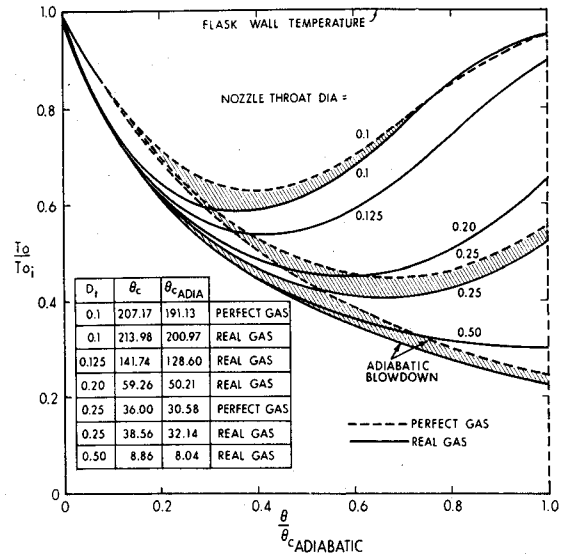

D_t	θ_c	$\theta_{c_{ADIA}}$	
0.1	207.17	191.13	PERFECT GAS
0.1	213.98	200.97	REAL GAS
0.125	141.74	128.60	REAL GAS
0.20	59.26	50.21	REAL GAS
0.25	36.00	30.58	PERFECT GAS
0.25	38.56	32.14	REAL GAS
0.50	8.86	8.04	REAL GAS

Fig. 1 Comparison of real-gas and perfect-gas predictions of flask air temperature for various nozzle throat diameters.

was computed from

$$T_{t,I+1} = T_{t,I} + [(T_{t,I-1} - T_{t,I})/(M_{t,I-1} - M_{t,I})](1 - M_{t,I}) \quad (14)$$

Equation (14) is applied on each pass through Eqs. (9–12, and A18) until the condition

$$|1 - M_t| < \epsilon \quad (15)$$

is satisfied. The flow rate from the reservoir may now be computed from $\dot{m}_0 = \rho_t A_t w_t$, and the throat pressure is found from $P_t = [1 + f_1(\rho_t, T_t)]RT_t\rho_t$. Then an evaluation of the time interval $\Delta\theta$ required to accomplish the flask changes may be made using $\dot{m}_0(\bar{\rho}_0, \bar{T}_0) = -\Delta m_0/\Delta\theta$, or

$$\Delta\theta = V_0[(\rho_0)_n - (\rho_0)_{n+1}]/\dot{m}_0(\bar{\rho}_0, \bar{T}_0) \quad (16)$$

Parametric Comparison of Real and Perfect Gas Solutions

Both the real gas and perfect gas analyses have been programed and run on an IBM 360-40. The numerical parameters used, unless otherwise specified, are as follows: $V_0 = 1.33$ ft^3, $P_{0i} = 4000$ psia, $T_{0i} = 80$°F, $h_i = 5$ Btu/hr-ft^2-°F, $D_t = 0.25$ in., $P_\infty = 14.7$ psia, $T_w = 80$°F, $m_w = 360$ lbm, $c_{pw} = 0.11$ Btu/lbm-°R, $A_i = 7.81$ ft^2, $R = 53.3$ ft-lbf/lbm-°R. The Beattie-Bridgeman equation of state was used in the real gas solutions

$$Z = 1 + \left(B - \frac{A}{RT} - \frac{C}{T^3}\right)\rho + \left(-bB + \frac{aA}{RT} - \frac{CB}{T^3}\right)\rho^2 + \frac{CbB}{T^3}\rho^3 \quad (17)$$

The numerical values of the constants A, a, B, b, and C were taken from Ref. 6 and T_w was treated as constant because its variation was small and had only a small effect on T_0.

Figure 1 shows the effect of D_t on $T_0(\theta)$ for both real gas and perfect gas. Three regimes are evident in the curves. In the first, gas expansion effects are dominant, and the temperature falls with time. In the second, thermal effects offset the expansion effects and the temperature reaches a minimum value. Finally, thermal effects dominate and T_0 rises toward T_w (= T_{0i}). Thermal effects are more significant at small D_t, and the minimum temperatures occur earlier in the nondimensionalized plane. The nondimensionalized coordinate system allows the temperature variations to be compared even though the total blowdown times are quite dissimilar. The adiabatic critical time $\theta_{c_{Adia}}$ (the time required for the flask pressure in an adiabatic blowdown to reach a value which just produces $M_t < 1$) is the reference value (denominator) for the abscissa. If instead, the actual critical time, which always exceeds $\theta_{c_{Adia}}$ because of the energy addition to the flask air, were used in the nondimensionalizing of the time, the temperature curves would be shifted slightly to the left and below their positions in Fig. 1 and would have appeared to give lower temperatures than in the adiabatic case.

The real gas temperatures (solid curves) are lower than the perfect gas temperatures, particularly near the minima. It is not simply high pressures which produce large differences in results, but rather the combination of high pressures and low temperatures. The lower left curves in Fig. 2 show, however,

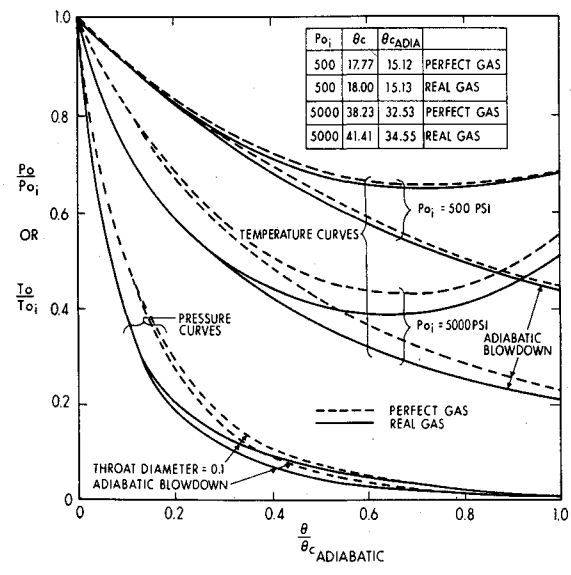

P_{o_i}	θ_c	$\theta_{c_{ADIA}}$	
500	17.77	15.12	PERFECT GAS
500	18.00	15.13	REAL GAS
5000	38.23	32.53	PERFECT GAS
5000	41.41	34.55	REAL GAS

Fig. 2 Comparison of real-gas and perfect-gas predictions showing effect of P_{oi} on T_o/T_{oi} and effect of D_t on P_o/P_{oi}.

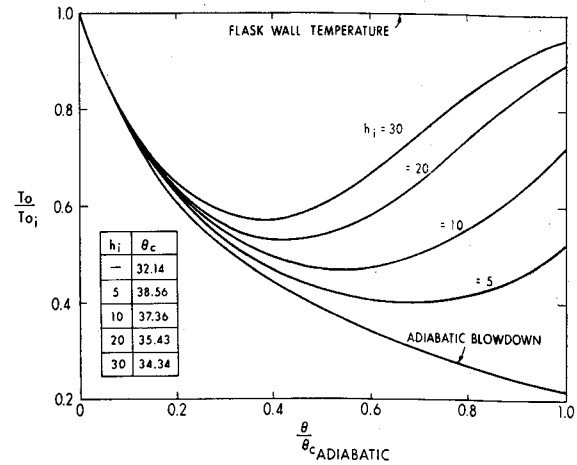

h_i	θ_c
—	32.14
5	38.56
10	37.36
20	35.43
30	34.34

Fig. 3 Flask air temperature predictions for various values of h_i.

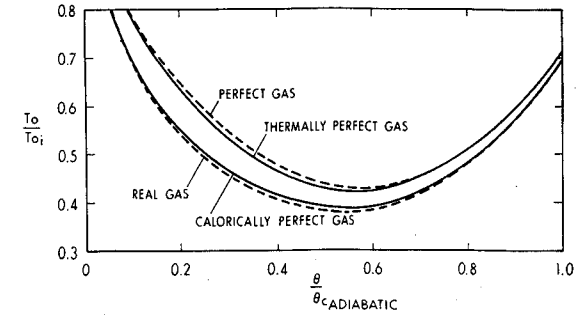

Fig. 4 Separate effects of caloric and thermal imperfections on T_0; P_{oi} = 5000 psi, h_i = 5 Btu/ft^2-hr-°F.

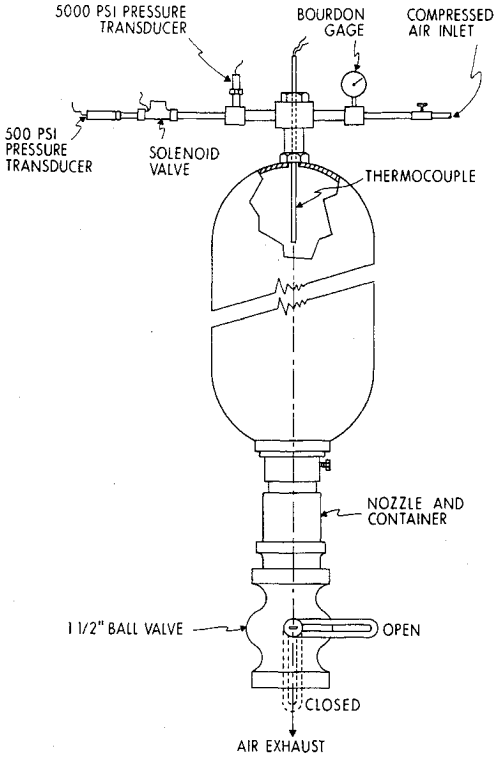

Fig. 5 Experimental apparatus used in the depressurization tests.

that the nondimensionalized pressure is quite insensitive to D_t, and that P_0 decreases to $\sim 0.4\ P_{0i}$ before there are any detectable thermal effects. The perfect gas solution indicates higher pressures than the real gas in the early stages of the blowdown. The effect of P_{0i} on the temperature ratios also can be seen from Fig. 2. The difference between the real and perfect gas solutions diminishes as P_{0i} is lowered, and for the specified conditions, it would appear that for $P_{0i} < 500$ psia, the perfect gas assumption should give acceptable predictions.

Figure 3 shows how the temperature varies when the heat transfer coefficient h_i is varied from the nominal 5 Btu/ft²-hr-°R used for Figs. 1 and 2. The similarity between this set of curves and those in Fig. 1 is striking. In fact, the curve for $h_i = 20$ Btu/ft²-hr-°F is almost identical to the real gas curve of Fig. 1 for $D_t = 0.125$ in.

Thermodynamically, a gas may be considered imperfect in two ways. If it does not obey the ideal gas equation, it is said to be thermally imperfect. If it does not have constant γ it is called calorically imperfect. By allowing all the virial coefficients to become zero, i.e., $Z = 1$, the gas is made thermally perfect. Figure 4 shows that the caloric imperfection is negligible.

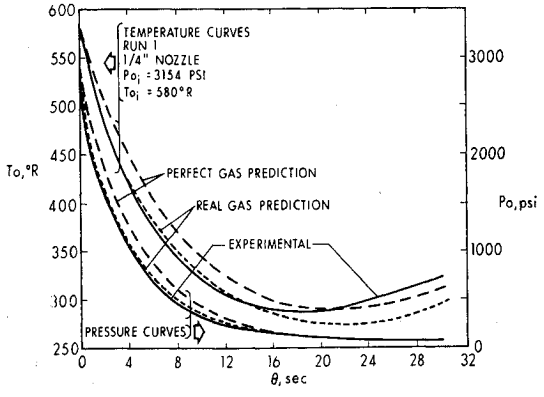

Fig. 6 Experimental results of depressurization through test nozzle with $\frac{1}{4}$-in. throat diameter; h_i from Eq. (18).

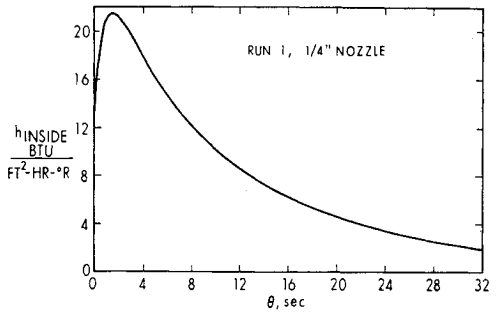

Fig. 7 h_i prediction.

Perhaps the largest error which is introduced into the analysis is due to the method of calculating h_i. Unfortunately, very little heat-transfer data exists for the range of pressure and Grashof number encountered here. To compare with the experimental study, h_i was calculated using the following empirical flat-plate formulas where the coefficients are taken from any standard heat transfer text, e.g., Ref. 7

$$h_i D_i/k_0 = \bar{c}\ X^{\bar{n}} \tag{18}$$

where $X = Gr_0 \cdot Pr_0$. The top half of the cylinder is taken as a heated plate facing downward, for which, with $3 \times 10^5 < X < 3 \times 10^{10}$, $\bar{c} = 0.27$ and $\bar{n} = \frac{1}{4}$; the bottom half of the cylinder is treated as a hot plate facing upward, for which, with $2 \times 10^7 < X < 3 \times 10^{10}$, $\bar{c} = 0.14$ and $\bar{n} = \frac{1}{3}$, and with $10^5 < X < 2 \times 10^7$, $\bar{c} = 0.54$ and $\bar{n} = \frac{1}{4}$. This procedure was used to calculate h_i by continuously evaluating the thermodynamic properties of the air throughout the blowdown.

Experimental Results

A 6000-psia, hydropneumatic accumulator, with its bladder removed, was used as the air cylinder. Its ends were modified to accommodate instrumentation and a nozzle insert (Fig. 5). The air was predried to avoid icing at the nozzle throat. The tank was charged to approximately the pressure desired, then several minutes were allowed for thermal mixing of the air in the cylinder. A test was initiated by hand actuation of the $1\frac{1}{2}$ in. ball valve. (This operation was fast enough to have a negligible effect in the blowdown.) Two conical nozzles, made of a laminated phenolic resin (trade name, Micarta) inside stainless-steel sleeves were used; their D_t's were $\frac{1}{4}$ in. and $\frac{3}{8}$ in. Two C.E.C. pressure transducers were used to measure P_{0i}. The 5000-psi transducer was allowed to record continuously throughout the blowdown while the 500-psi transducer was prevented from "seeing" P_{0i} by use of a closed solenoid valve until P_{0i} had diminished to ~ 100 psi. To obtain the desired fast response for T_{0i}, an exposed-junction, BLH microminiature, copper-constantan thermocouple (bead diameter ~ 0.002 in.) was used. The larger thermocouple lead wires were encased in a $\frac{1}{8}$-in. stainless-steel tube sealed with epoxy.

A total of 15 runs were made, with $2000 \leq P_{0i} \leq 4000$ psi, in the open air, so that climatic changes did have some effect on T_{0i}. Results from a test with the $\frac{1}{4}$-in. throat nozzle are compared with predictions in Fig. 6. (The differences between experimental results and calculated values were approximately the same for all runs with a given nozzle size.) The real-gas, pressure-time predictions are in close agreement with the experimental values, and are, as expected at these high pressures, superior to the perfect-gas calculated values. The temperature-time predictions are rather disappointing, especially near the end of the run.

In the early blowdown stages, the real-gas solution tends to overestimate the temperature in the $\frac{1}{4}$-in.-nozzle calculations, but is conservative by a similar small amount (not shown) for the $\frac{3}{8}$-in. nozzle. As mentioned earlier, the h_i calculation (Fig. 7) is rather crude. Although a major share of the difference between experiment and calculation may be

blamed on poor h_i estimation, some of the error is undoubtedly due to the following idealizations in the mathematical model: treatment as a "quasi"-steady process; isentropic flow in the nozzle (which of course means the nozzle has a discharge coefficient of unity and a zero over-all loss coefficient); all flask temperature and pressure gradients were neglected; use of the Beattie-Bridgeman equation; and use of the finite differencing scheme. With respect to the experiment, the thermocouple must be capable of following a temperature which can drop at almost 100°F/sec in a relatively stagnant medium. This is a rather difficult task even for the smallest of thermocouples. The manufacturer's data states that the thermocouple used in the tests requires about 13 msec to reach 63.2% of an imposed step change in temperature for a flow velocity of 65 fps. Clearly, as this velocity is diminished, the time required for the same temperature variation will rise. Thus, in the early portion of the blowdown, differences can be attributed to the thermocouple lag. No precaution was taken to avoid radiation heat-transfer interchange between the thermocouple and the wall; a rough steady-state analysis shows that the temperature correction for radiation is large enough to account for the differences in temperatures toward the end of the blowdown.

Appendix

The following stems from the work of Johnson,[5,6] let:

$$Z = Z(\rho,T) = 1 + \sum_{i=1}^{I} A_i(T)\rho^i = 1 + \sum_i \left(\sum_{j=0}^{J} a_{ij}/T^j\right)\rho^i \quad \text{(A1)}$$

then

$$f_1(\rho,T) \equiv Z - 1 = \sum_i A_i(T)\rho^i \quad \text{(A2)}$$

$$f_2(\rho,T) \equiv T(\partial Z/\partial T)_\rho = -\sum_i \sum_j j(a_{ij}/T^j)\rho^i \quad \text{(A3)}$$

$$f_3(\rho,T) \equiv Z - 1 + \rho(\partial Z/\partial\rho)_T = \sum_i (1+i)A_i(T)\rho^i \quad \text{(A4)}$$

$$f_4(\rho,T) \equiv \int_0^\rho \left[Z - 1 + T\left(\frac{\partial Z}{\partial T}\right)_\rho\right]\frac{d\rho}{\rho} = \sum_i \sum_j (j-1)\left(\frac{a_{ij}}{T^j}\right)\left(\frac{\rho^i}{i}\right) \quad \text{(A5)}$$

$$f_5(\rho,T) \equiv \int_0^\rho f_2(\rho,T)\frac{d\rho}{\rho} = -\sum_i \sum_j j\left(\frac{a_{ij}}{T^j}\right)\rho^i \quad \text{(A6)}$$

$$f_6(\rho,T) \equiv T(\partial f_4/\partial T)\rho = \sum_i \sum_j (j-1)j(a_{ij}/T^j)(\rho^i/i) \quad \text{(A7)}$$

$$g_1(T_2,T_1) \equiv \int_{T_1}^{T_2}\left(\frac{c_{p,0}}{R} - 1\right)\frac{dT}{T} = (c_0 - 1)\ln\left(\frac{T_2}{T_1}\right) + \sum_{k=1}^{K}\left(\frac{c_k}{k}\right)(T_2{}^k - T_1{}^k) \quad \text{(A8)}$$

$$g_2(T_2,T_1) \equiv \int_{T_1}^{T_2}\left(\frac{C_{p0}}{R} - 1\right)dT = (c_0 - 1)(T_2 - T_1) + \sum c_k\frac{(T_2{}^k - T_1{}^k)}{(k+1)} \quad \text{(A9)}$$

$$g_3(T_2,T_1) \equiv \int_{T_1}^{T_2}\left(\frac{c_{p,0}}{R}\right)\frac{dT}{T} = g_1(T_2,T_1) + \ln\left(\frac{T_2}{T_1}\right) \quad \text{(A10)}$$

where

$$\frac{c_{p,0}(T)}{R} = c_0 + \sum_{k=1}^{K} c_k T^k \quad \text{(A11)}$$

Integrating first along a path of constant T_1 then along a path of constant ρ and finally along a constant T_2 we may write

$$(s_2 - s_1)/R = \int_{1\to2}\{(c_vT)/(RT) - [Z + T(\partial Z/\partial T)_\rho]d\rho/\rho\} = g_1(T_2,T_1) + \ln(\rho_1/\rho_2) - f_4(\rho_2,T_2) + f_4(\rho_1,T_1) \quad \text{(A12)}$$

$$(u_2 - u_1)/R = \int_{1\to2}[(c_vdT)/(RT) - T^2(\partial Z/\partial T)_\rho d\rho/\rho = g_2(T_2,T_1) + T_1f_5(\rho_1,T_1) - T_2f_5(\rho_2,T_2) \quad \text{(A13)}$$

$$(h_2 - h_1)/R = (u_2 - u_1)/R + P_2/(\rho_2R) - P_1/(\rho_1R) = (u_2 - u_1)/R + Z_2T_2 - Z_1T_1 \quad \text{(A14)}$$

furthermore

$$c_v/R = T(\partial s/\partial T)_\rho/R = c_{p,0}/R - 1 - f_6(\rho_1T) \quad \text{(A15)}$$

$$c_p/R = c_v/R - T(\partial s/\partial\rho)_T(\partial\rho/\partial T)_\rho/R = c_v/R + (1 + f_1 + f_2)^2/(1 + f_3) \quad \text{(A16)}$$

$$\gamma = (c_p/R)/(c_v/R) \quad \text{(A17)}$$

$$a^2 = (\partial P/\partial\rho)s = (\partial P/\partial\rho)_T + (\partial P/\partial T)_\rho(\partial T/\partial\rho)s = [1 + f_3 + (1 + f_1 + f_2)^2/(c_{p,0}/R - 1 - f_6)]RT \quad \text{(A18)}$$

References

[1] Reynolds, W. C. and Kays, W. M., "Blowdown and Charging Processes in a Single Gas Receiver with Heat Transfer," *Transactions of the ASME*, Vol. 80, 1958, pp. 1160–1168.

[2] Tsien, H. S., "One Dimensional Flows of a Gas Characterized by van der Waal's Equation of State," *Journal of Math and Physics*, Vol. 25, No. 6, 1947, pp. 301–324.

[3] Tao, L. N., "Gas Dynamic Behavior of Real Gases," *Journal of Aero Sciences*, Nov. 1955, pp. 763–774 and 794.

[4] Johnson, R. C., "Calculation of Real-Gas Effects in Flow Through Critical-Flow Nozzles," *Transactions of the ASME: Journal of Basic Engineering*, Sept. 1964, pp. 519–526.

[5] Johnson, R. C., "Real-Gas Effects in Critical-Flow-Through Nozzles and Tabulated Thermodynamic Properties," TN D-2565, Jan. 1965, NASA.

[6] Hilsenrath, J. et al., *Tables of Thermodynamic and Transport Properties*, Pergamon Press, New York, 1960 (NBS Circular 564).

[7] McAdams, W. H., *Heat Transmission*, 3rd ed., McGraw-Hill, New York, 1954, p. 180.

Effect of Orifice Length-to-Diameter Ratio on Mixing in the Spray from a Pair of Unlike Impinging Jets

ROBERT W. RIEBLING*

Jet Propulsion Laboratory, Pasadena, Calif.

Nomenclature

d = orifice diameter

$$E_m = 1 - \left[\left(\sum_0^n c\dot{w}_t(R - r)\Big/\dot{W}_tR\right) + \left(\sum_0^{\bar{n}} c\dot{w}_t(R - \bar{r})\Big/\dot{W}_t(R - 1)\right)\right],$$

Received February 16, 1970; revision received April 1, 1970.

This paper presents the results of one phase of research carried out at the Jet Propulsion Laboratory, California Institute of Technology, under Contract NAS 7-100, sponsored by NASA.

* Supervisor, Combustion Devices Development Group, Liquid Propulsion Section; also Instructor, Engineering Extension, University of California at Los Angeles. Member AIAA.